Experimental study of the spectroscopic factors of $^{116-125}$Sn

L. Gan,[1,2] H. B. Sun,[2,*] Z. H. Li,[3,†] S. P. Hu,[2] Y. J. Li,[3] J. Su,[3] B. Guo,[3] S. Q. Yan,[3] Y. B. Wang,[3] S. Zeng,[3] Z. Y. Han,[3] X. Y. Li,[3] D. H. Li,[3] T. L. Ma,[3] Y. P. Shen,[3] Y. Su,[3] E. T. Li,[2] and W. P. Liu[3]

[1]*Key Laboratory of Optoelectronic Devices and Systems of Ministry of Education and Guangdong Province, College of Optoelectronic Engineering, Shenzhen University, Shenzhen 518060*

[2]*College of Physics and Optoelectronic Engineering, Shenzhen University, Shenzhen 518060, China*

[3]*China Institute of Atomic Energy, P.O. Box 275(10), Beijing 102413, China*

(Received 8 July 2019; revised manuscript received 30 November 2019; published 21 January 2020)

Enriched targets of $^{116,118,120,122,124}SnO_2$ were bombarded with proton and deuteron beams, and the angular distributions of (p,d) and (d,p) on tin isotopes were accurately measured using the high-precision Q3D magnetic spectrograph at the Beijing HI-13 tandem accelerator of the China Institute of Atomic Energy. Distorted-wave Born approximation calculations were performed to extract the neutron spectroscopic factors (SFs) using two different sets of systematic optical potential parameters for these neutron transfer reactions. The SFs of $^{116-125}$Sn were obtained and compared to previous values. Our results are consistent with the average of the previous data within the error range. It is worth noting that the reaction products corresponding to $^{119}Sn_{G.S.}$ and $^{119}Sn^*_{0.024}$, to $^{123}Sn_{G.S.}$ and $^{123}Sn^*_{0.025}$, and to $^{125}Sn_{G.S.}$ and $^{125}Sn^*_{0.028}$ were first distinguished by the present experiment; therefore, our results of the low lying states of ^{119,123,125}Sn are more reliable. However, the first excited state of ^{121}Sn is only 0.006 MeV; we failed to identify the products that correspond to the ground state and the first excited state, and the extracted SFs of $^{120}Sn_{G.S.} \otimes n \rightarrow {}^{121}Sn_{0.006.}$ and $^{121}Sn_{0.006} \otimes n \rightarrow {}^{122}Sn_{G.S}$ are not reliable. A simple linear formula was used to analyze the relationship of SFs with neutron separation energy $S_n(N)$ and the even-A Sn pairing gap $\Delta(N)$, and SFs are found to be positively correlated to $S_n(N)$ and $\Delta(N)$.

DOI: 10.1103/PhysRevC.101.014612

I. INTRODUCTION

For more than fifty years, the nuclear shell model has played a crucial role in explaining nuclear properties in the region of low excitation energy [1,2]. The tin isotopes are extremely suitable to provide information about the 50–82 neutron shell, due to the proton number being the magic number 50. This closed shell structure of protons greatly reduces the ambiguities caused by the neutron-proton residual interaction, making the neutron spectrum relatively simple, so that theoretical calculations are much more reliable [3–9]. In addition, this strong closure proton shell, leading to the existence of ten stable tin isotopes ^{112,114,116,117,118,119,120,122,124}Sn, allows us to carry out a systematic study.

The spectroscopic factor (SF), which is decided by the wave functions of the entrance channel and exit channel, provides quantitative information about the single-particle structure of nuclei in the shell model [10,11]. Transfer reactions, especially one-nucleon transfer reactions, have been widely used to gather information for the shell model of nuclear structure [3,4]. One can obtain spectroscopic information through one-nucleon transfer reactions. The angular distribution of transfer reactions permits the extraction of spectroscopic factors by using theoretical models, the most common model being the distorted-wave Born approximation (DWBA) theory.

Stripping and capture reactions have been widely applied to shell-model studies of nuclear structure [3]. These transfer reactions allow the population of various excited states via different experimental sets. The use of the DWBA theory for the description of (d,p) and (p,d) reactions has contributed considerably to the extraction of the spectroscopic factors of tin isotopes in the past half century. However, the previous works were too old or concerned just a few tin isotopes, so a systematic study was needed. On the other hand, due to the low excited energy of the first excited states of ^{119}Sn (0.024 MeV), ^{121}Sn (0.006 MeV), ^{123}Sn (0.025 MeV), and ^{125}Sn (0.028 MeV), all of the previous work failed to clearly identify the reaction products of the ground states with the first excited states of these nuclides. For example, for the ground state of ^{120}Sn, the results from ^{119}Sn capturing a neutron (1.3 to 1.8) are significantly larger than that from ^{120}Sn losing a neutron (0.58). This large difference is likely to come from the interference of the first excited state of ^{119}Sn. In addition, ^{121}Sn ($t_{1/2} = 27.0$ h), ^{123}Sn ($t_{1/2} = 129.2$ d), and ^{125}Sn ($t_{1/2} = 9.6$ d) are unstable; the SFs of $^{121-125}$Sn in previous work were extracted by capturing or losing a neutron by ^{120,122,124}Sn. Therefore, the deduced neutron spectroscopic factors tend to be unreliable. In order to extract the exact SFs of $^{121-125}$Sn, new experimental measurement with higher precision should be performed.

In this work, the neutron spectroscopic factors of $^{116-125}$Sn were extracted through measuring the angular distributions of

*hbsun@szu.edu.cn
†zhli@ciae.ac.cn

TABLE I. Isotopic abundances and thicknesses of tin targets.

Isotope	Abundance (%)	Thickness (μg/cm^2)
^{116}Sn	95.52 ± 0.10	77.2 ± 5.4
^{118}Sn	96.70 ± 0.05	30.0 ± 2.2
^{120}Sn	98.31 ± 0.04	48.0 ± 3.9
^{122}Sn	92.11 ± 0.05	59.4 ± 4.1
^{124}Sn	96.32 ± 0.05	64.6 ± 4.6

(p, d) and (d, p) reactions on ^{116,118,120,122,124}Sn, and the previous work can be used as a consistency check of the extracted spectroscopic factors. The experiments were performed with the Q3D magnetic spectrograph at the HI-13 tandem accelerator of the China Institute of Atomic Energy (CIAE), Beijing. The Q3D magnetic spectrograph has a high energy resolution of about 0.02%, and the angular distributions can be measured with high precision.

II. EXPERIMENT

According to the accelerator beam arrangement, the experimental measurements were divided into two parts: $^{116,118,120}SnO_2$ were bombarded with 18.0 MeV proton and 12.0 MeV deuterium beams; $^{122,124}SnO_2$ were bombarded with 14.0 MeV proton and 12.0 MeV deuterium beams. The isotopic abundances and thicknesses of the ^{116,118,120,122,124}Sn are listed in Table I, and were calibrated by the $^{12}C + {}^{116,118,120,122,124}$Sn elastic scattering cross sections of front angles to the Rutherford scattering cross sections at 60 MeV.

The angular distributions of (p, d) and (d, p) neutron transfer reactions on $^{116,118,120,122,124}SnO_2$ were measured with the experimental setup shown in Fig. 1. The proton and deuteron beams from the accelerator impinged on the self-supported tin enriched isotope targets of SnO_2. The self-supported targets were set at the center of the target chamber, and the diameter of target chamber is 479 mm. The ejected particles entered the Q3D magnetic spectrometer through a diaphragm with an accepted solid angle of 0.34 ± 0.01 msr for excellent angular resolution. To count the incoming particles, a movable Faraday cup was placed behind the reaction targets.

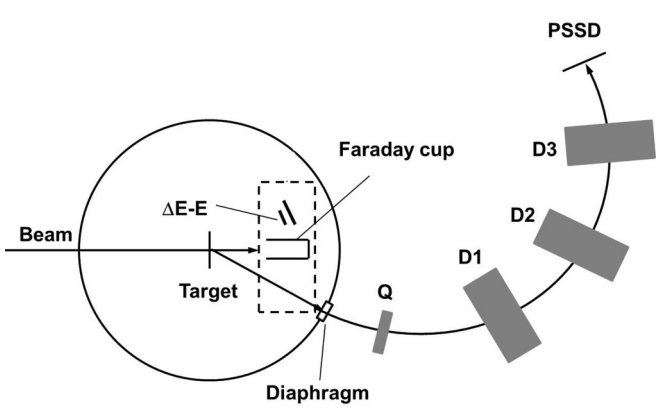

FIG. 1. Experimental setup.

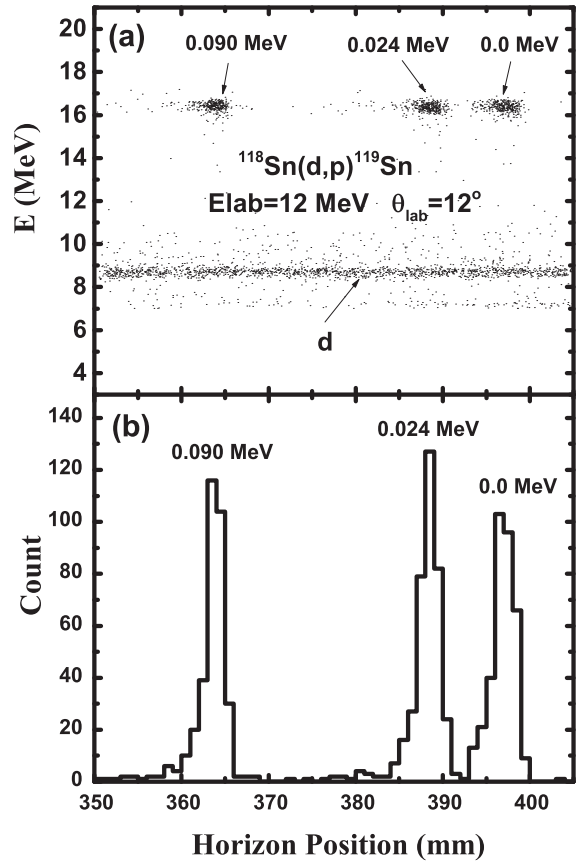

FIG. 2. The two-dimensional spectrum of kinetic energy versus the horizon position (a) and the horizon position spectrum of object ions (b) for ^{118}Sn(d, p) ^{119}Sn at 12°.

For the purpose of cross-checking the beam intensity, a ΔE-E detector telescopic system was set at about 23° downstream of the reaction targets. The reaction products were separated according to the difference between energy and charge-to-mass ratio by Q3D, and then energy and horizontal position information were recorded by a 50 mm × 50 mm two-dimensional position-sensitive silicon detector (PSSD) at the focal plane. Most of the ions from other reaction channels can be excluded by the magnetic field of Q3D, and the position-energy information measured by PSSD enable us to pick out the object ions from remaining particles.

Figure 2(a) shows the typical two-dimensional spectrum of kinetic energy versus the horizon position for the ^{118}Sn(d, p) ^{119}Sn reaction at 12°. It can be seen that the protons from ^{118}Sn(d, p) ^{119}Sn can be clearly identified according to the energy information, and the reaction products from different excited states can be accurately counted through the position spectrum of object ions, as shown in Fig. 2(b).

III. DWBA CALCULATIONS

The experimental cross sections were analyzed with DWBA calculations. This procedure supports the extraction of the spectroscopic factors by taking the ratios of the experimental cross sections to the predicted cross sections. The

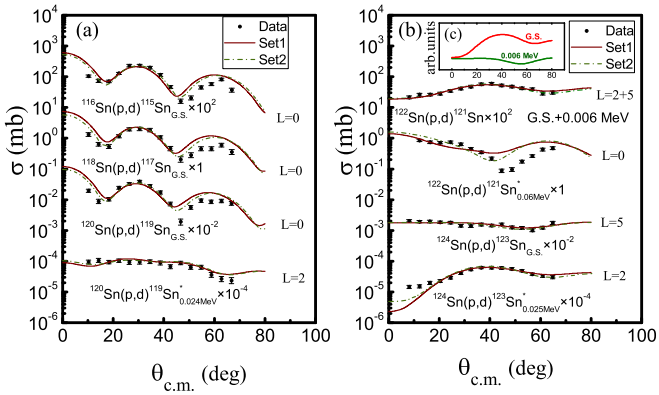

FIG. 3. The angular distributions of differential cross sections of ^{116,118,120}Sn(p,d) and ^{122,124}Sn(p,d) are shown in (a) and (b), respectively. The red solid curves are from the normalized DWBA calculation by set 1, the green dashed curves represent the results of set 2, while dots are experimental distributions. The calculated curves of ^{122}Sn(p,d) ^{121}Sn$_{\mathrm{G.S.}+0.006}$ in (b) were mathematically fitted with the DWBA calculations for Sn$_{\mathrm{G.S.}}$ and Sn$^{*}_{0.006}$. Panel (c) shows the DWBA angular distributions of ^{122}Sn(p,d) ^{121}Sn$_{\mathrm{G.S.}}$ (red curve) and ^{122}Sn(p,d) ^{121}Sn$_{0.006}$ (green curve).

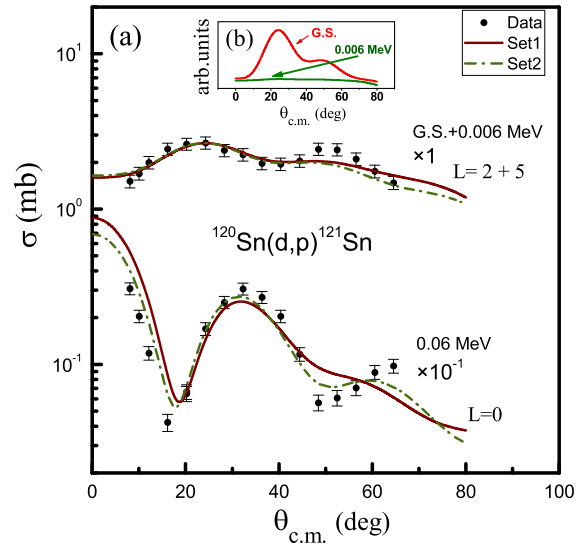

FIG. 5. The angular distributions of differential cross sections of ^{120}Sn(d,p) ^{121}Sn. The calculated curves of ^{120}Sn$(d,p)^{121}$Sn$_{\mathrm{G.S.}+0.006}$ in (a) were mathematically fitted with the DWBA calculations for Sn$_{\mathrm{G.S.}}$ and Sn$^{*}_{0.006}$. The theoretical shapes of ^{120}Sn(d,p) ^{121}Sn$_{\mathrm{G.S.}}$ and ^{120}Sn$(d,p)^{121}$Sn$^{*}_{0.006}$ are shown in (b).

equation can be expressed as [12,13]

$$\mathrm{SF} = \frac{d\sigma_{\mathrm{exp}}/d\Omega}{d\sigma_{\mathrm{DWBA}}/d\Omega}, \tag{1}$$

where $d\sigma_{\mathrm{exp}}/d\Omega$ and $d\sigma_{\mathrm{DWBA}}/d\Omega$ are the experimental and DWBA theoretical differential cross sections of the transfer reaction, respectively.

The geometrical parameters of radius and diffuseness for the single-particle bound state were chosen to be 1.25 fm and 0.65 fm, respectively. The transfer reaction calculations were carried out using the code TWOFNR [14], which is convenient for calculating (p,d), (n,d), $(d,{}^{3}\mathrm{He})$ and their reverse reactions with finite range or zero range, and finite range was adopted in this work. In order to analyze the influence of the optical potential, two sets of optical potential parameters were adopted: The optical potential for deuterons used the Lohr-Haeberli [15] global optical model potentials (OMPs) and the optical potential for protons used the Chapel-Hill 89 [16] global OMPs (set 1) and Perey [17] global OMPs (set 2). Figuress 3–6 present the results of DWBA calculations for ^{116,118,120,122,124}Sn(p,d) and (d,p) reactions with red solid curves (set 1) and green dashed curves (set 2). One can see that most of the curves can reproduce the experimental data well. There are about 40 reaction channels, and each $d + {}^{A}$Sn channel has two optical potential parameter sets. The formulas of global OMPs are given in the Appendix instead of listing the values of optical potential parameters.

The neutron spectroscopic factors extracted in the present work are summarized in Tables II and III. The SFs of $^{116\text{–}125}$Sn were obtained with two values. The uncertainties of the spectroscopic factors are contributed by the experimental errors (statistics errors and the target thickness uncertainties, about 10% in all) and the influence of the optical parameters (from 6% to 20%). It is worth noting that the experimental platform

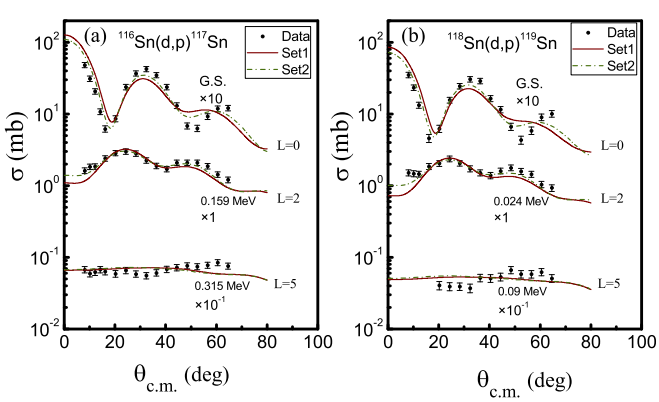

FIG. 4. The angular distributions of differential cross sections of ^{116}Sn(d,p) ^{117}Sn (a) and ^{118}Sn(d,p) ^{119}Sn (b).

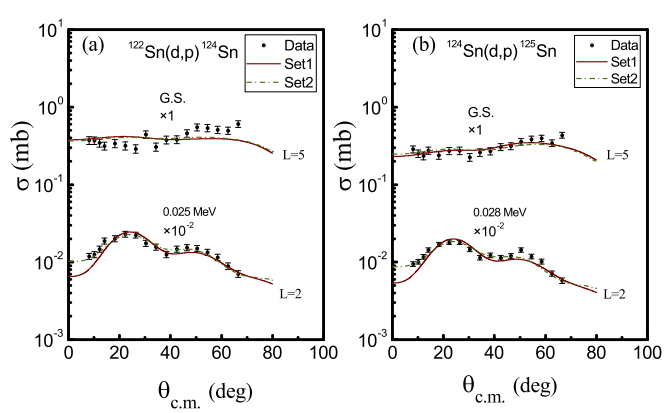

FIG. 6. The angular distributions of differential cross sections of ^{122}Sn(d,p) ^{123}Sn (a) and ^{124}Sn(d,p) ^{125}Sn (b).

TABLE II. Spectroscopic factors of ^{116,118,120,122,124}Sn by ^{A}Sn(p,d) $^{A-1}$Sn. L represent single-particle orbital angular momentum.

Transition	$^{A-1}$Sn	E^* (MeV)	J^π	L	Set 1	Set 2	Average
^{116}Sn(p,d)	^{115}Sn	0	$1/2^+$	0	1.13 ± 0.11	0.95 ± 0.09	1.04 ± 0.13
^{118}Sn(p,d)	^{117}Sn	0	$1/2^+$	0	1.12 ± 0.14	0.85 ± 0.11	0.99 ± 0.18
^{120}Sn(p,d)	^{119}Sn	0	$1/2^+$	0	1.53 ± 0.18	1.22 ± 0.15	1.38 ± 0.22
		0.024	$1/2^+$	2	1.49 ± 0.21	1.22 ± 0.17	1.36 ± 0.24
^{122}Sn(p,d)	^{121}Sn	0	$3/2^+$	2	1.80 ± 0.18	1.38 ± 0.14	1.59 ± 0.26
		0.060	$1/2^+$	0	2.01 ± 0.20	1.54 ± 0.15	1.77 ± 0.29
^{124}Sn(p,d)	^{123}Sn	0	$11/2^-$	5	7.17 ± 0.71	5.35 ± 0.53	6.26 ± 1.10
		0.025	$3/2^+$	2	2.20 ± 0.21	1.58 ± 0.15	1.89 ± 0.36

in the present work has much better resolution capability than those in the previous works, so we can distinguish the reactions products of adjacent energy levels, such as ^{119}Sn$_{\text{G.S.}}$ and ^{119}Sn$^*_{0.024}$. The first exited state of ^{121}Sn is only 6 keV; we failed to distinguish the products of ^{121}Sn$_{\text{G.S.}}$ and ^{121}Sn$^*_{0.006}$ in ^{120}Sn(d,p) ^{121}Sn and ^{122}Sn(p,d) ^{121}Sn reactions. But it can be seen in Figs. 3(c) and 5(b) that the the peaks of both ^{122}Sn(p,d) ^{121}Sn$_{\text{G.S.}}$ +0.006 and ^{120}Sn(d,p) ^{121}Sn$_{\text{G.S.}}$ +0.006 are only contributed by the ground state, so that the SFs of ^{120}Sn$_{\text{G.S.}} \otimes n \rightarrow$ ^{121}Sn$_{\text{G.S.}}$ and ^{121}Sn$_{\text{G.S.}} \otimes n \rightarrow$ ^{122}Sn$_{\text{G.S.}}$ are trustworthy. Oppositely, the SFs corresponding to ^{121}Sn$_{0.006}$ are unreliable: the SFs of ^{120}Sn$_{\text{G.S.}} \otimes n \rightarrow$ ^{121}Sn$_{0.006}$ are 1.27 ± 0.12 (set 1) and 0.66 ± 0.06 (set 2), and the SFs of ^{121}Sn$_{0.006.} \otimes n \rightarrow$ ^{122}Sn$_{\text{G.S.}}$ are 4.99 ± 0.49 (set 1) and 7.62 ± 0.75 (set 2).

The comparisons of the SFs obtained from the present work with those from the previous works are listed in Tables IV–XIII and shown in Figs. 7–11. The error bars of the present work are larger than those of some previous work. This is because many previous works did not give the errors of SFs, or just gave the statistical errors. However, the present results considered not only the experimental errors (statistical errors and target thickness uncertainties) but also the influence of optical potential.

Figure 12 shows the tendency of SFs versus single neutron separation energy $S_n(N)$. Obviously, the SFs corresponding to 8–10 MeV (even-A Sn isotopes) are much larger than 5–7 MeV (odd-A Sn isotopes) for each L. In addition SFs in the range 5–7 MeV show an increasing tendency with increasing $S_n(N)$, but those in 8–10 MeV indicate an opposite phenomenon. It is well understood for us that SFs grow with increasing $S_n(N)$. We think the pairing correlation of even-A Sn isotopes produces this abnormal phenomenon. To estimate the influence of pairing correlation in even-A Sn isotopes, three- [39,41], four- [39,41], and five-point [40,41] formulas of pairing gap Δ were used in this work:

$$\Delta_n^{(3)}(N) = -\tfrac{1}{2}[S_n(N+1) - S_n(N)], \tag{2}$$

$$\Delta_n^{(4)}(N) = -\tfrac{1}{4}[S_n(N+1) - 2S_n(N) + S_n(N-1)], \tag{3}$$

$$\Delta_n^{(5)}(N) = -\tfrac{1}{8}[3S_n(N+1) - 3S_n(N) + S_n(N-1) - S_n(N-2)]. \tag{4}$$

It seams that SFs show a linear relationship with neutron separation energy $S_n(N)$ and pairing gap $\Delta(N)$, as shown in Fig. 12 and Table XIV. Thus, we applied a simple linear fitting for each L with the form $\text{SF} = a_0 \times S_n(N) + a_1 \times \Delta(N)$, and the result are shown in Fig. 12. The calculated data points were connected with lines to present the fitting effect to the SFs. The values of a_0 and a_1 of each L are listed in Table XV. We can see that the parameters obtained using $\Delta_n^{(3)}(N)$, $\Delta_n^{(4)}(N)$, and $\Delta_n^{(5)}(N)$ are similar. All of the a_0's and a_1's are positive, which means SFs are positively correlated to $S_n(N)$ and $\Delta(N)$. For $L =$ 0, 2, and 5, a_0 has similar values. But for $L = 5$, a_1 is

TABLE III. Spectroscopic factors of ^{117,119,121,123,125}Sn by ^{A}Sn(d,p) $^{A+1}$Sn. L represent single-particle orbital angular momentum.

Transition	$^{A+1}$Sn	E^* (MeV)	J^π	L	Set 1	Set 2	Average
^{116}Sn(d,p)	^{117}Sn	0	$1/2^+$	0	0.71 ± 0.06	0.62 ± 0.06	0.67 ± 0.08
		0.159	$3/2^+$	2	0.93 ± 0.08	0.82 ± 0.07	0.88 ± 0.09
		0.315	$11/2^-$	5	0.81 ± 0.08	0.64 ± 0.06	0.73 ± 0.11
^{118}Sn(d,p)	^{119}Sn	0	$1/2^+$	0	0.45 ± 0.05	0.38 ± 0.05	0.42 ± 0.06
		0.024	$3/2^+$	2	0.65 ± 0.06	0.58 ± 0.06	0.62 ± 0.07
		0.090	$11/2^-$	5	0.49 ± 0.06	0.37 ± 0.05	0.43 ± 0.06
^{120}Sn(d,p)	^{121}Sn	0	$3/2^+$	0	0.33 ± 0.03	0.40 ± 0.04	0.37 ± 0.05
		0.060	$1/2^+$	0	0.48 ± 0.05	0.40 ± 0.04	0.44 ± 0.06
^{122}Sn(d,p)	^{123}Sn	0	$11/2^-$	5	0.46 ± 0.05	0.33 ± 0.03	0.40 ± 0.07
		0.025	$3/2^+$	2	0.58 ± 0.05	0.51 ± 0.05	0.55 ± 0.06
^{124}Sn(d,p)	^{125}Sn	0	$11/2^-$	5	0.36 ± 0.04	0.25 ± 0.03	0.31 ± 0.07
		0.028	$3/2^+$	0	0.44 ± 0.03	0.39 ± 0.03	0.42 ± 0.04

TABLE IV. Comparison of the neutron spectroscopic factors of ^{115}Sn ⊗n → ^{116}Sn$_{G.S.}$.

Ref.	E^*_{115Sn} (MeV)	SF	Reaction	E_{Lab} (MeV)
[3]	0	1.08	^{115}Sn(d,p)	15
[7]	0	1.00 ± 0.10	^{116}Sn(p,d)	20
[18]	0	0.53 ± 0.11	^{116}Sn(d,t)	55
[19]	0	0.70 ± 0.07	^{116}Sn(d,t)	23
[20]	0	0.82	Weak-coupling calculation	
[21]	0	0.75 ± 0.08	^{116}Sn(pol d,t)	40
present	0	1.04 ± 0.13[a]	^{116}Sn(p,d)	18

[a]Average value.

TABLE V. Comparison of the neutron spectroscopic factors of ^{116}Sn$_{G.S.}$ ⊗n → ^{117}Sn.

Ref.	E^*_{117Sn} (MeV)	SF	Reaction	E_{Lab} (MeV)
[1]	0	0.45 ± 0.07	^{117}Sn(p,d)	55
[3]	0	0.65	^{116}Sn(d,p)	15
[3]	0.159	0.55	^{116}Sn(d,p)	15
[3]	0.315	0.81	^{116}Sn(d,p)	15
[7]	0	0.65 ± 0.08	^{117}Sn(p,d)	20
[22]	0	0.76	^{116}Sn$(\alpha,\ ^3$He$)$	65.7
[22]	0.159	0.45[a]	^{116}Sn$(\alpha,\ ^3$He$)$	65.7
[22]	0.315	0.69[a]	^{116}Sn$(\alpha,\ ^3$He$)$	65.7
[23]	0	0.52 ± 0.08	^{116}Sn(d,p)	4.5–5.5
[23]	0.159	0.76 ± 0.114	^{116}Sn(d,p)	4.5–5.5
[23]	0.315	0.79 ± 0.12	^{116}Sn(d,p)	4.5–5.5
[24]	0	0.62 ± 0.20[a]	^{116}Sn(pol d,p)	8.22
[24]	0.159	0.83 ± 0.22[a]	^{116}Sn (pol d,p)	8.22
[24]	0.315	0.66 ± 0.17[a]	^{116}Sn(pol d,p)	8.22
[25]	0	0.7	^{116}Sn(d,p)	79
[25]	0.159	0.7	^{116}Sn(d,p)	79
[25]	0.315	0.3	^{116}Sn(d,p)	79
[26]	0	0.64 ± 0.128	^{117}Sn(d,t)	50
[27]	0	0.53	^{116}Sn(t,d)	4.25–5.75
[27]	0.159	0.52	^{116}Sn(t,d)	4.25–5.75
[27]	0.315	0.9	^{116}Sn(t,d)	4.25–5.75
present	0	0.67 ± 0.08[a]	^{116}Sn(d,p)	12
present	0.159	0.88 ± 0.09[a]	^{116}Sn(d,p)	12
present	0.315	0.58 ± 0.09[a]	^{116}Sn(d,p)	12

[a]Average value.

TABLE VI. Comparison of the neutron spectroscopic factors of ^{117}Sn ⊗n → ^{118}Sn$_{G.S.}$.

Ref.	E^*_{117Sn} (MeV)	SF	Reaction	E_{Lab} (MeV)
[3]	0	1.40	^{117}Sn(d,p)	15
[4]	0	1.40 ± 0.14	^{118}Sn(pol p,d)	21
[7]	0	1.40 ± 0.15	^{118}Sn(p,d)	20
[8]	0	0.90	^{117}Sn(d,p)	12
[27]	0	1.40	^{117}Sn(t,d)	4.75–5.75
[28]	0	1.10 ± 0.17	^{118}Sn(p,d)	55
[29]	0	1.30	^{118}Sn(p,d)	24.95
[30]	0	1.31 ± 0.26	^{118}Sn(pol d,t)	12
[31]	0	1.37	^{117}Sn(pol d,p)	12
[32]	0	1.47 ± 0.29	^{118}Sn(pol p,d)	22
present	0	0.99 ± 0.18[a]	^{118}Sn(p,d)	18

[a]Average value.

TABLE VII. Comparison of the neutron spectroscopic factors of ^{118}Sn$_{G.S.}$ ⊗n → ^{119}Sn.

Ref.	E^*_{119Sn} (MeV)	SF	Reaction	E_{Lab} (MeV)
[3]	0	0.59	^{118}Sn(d,p)	15
[3]	0.024	0.52	^{118}Sn(d,p)	15
[3]	0.09	0.56	^{118}Sn(d,p)	15
[7]	0	0.55 ± 0.05	^{119}Sn(p,d)	20
[9]	0.09	0.35 ± 0.04	^{118}Sn$(\alpha,\ ^3$He$)$	187
[27]	0	0.37	^{118}Sn(t,d)	4.5–5.75
[27]	0.024	0.44	^{118}Sn(t,d)	4.5–5.75
[27]	0.09	0.85	^{118}Sn(t,d)	5.5–5.75
[33]	0	0.45	^{119}Sn(p,d)	55
[34]	0	0.29 ± 0.07	^{118}Sn(d,p)	17
[34]	0.024	0.52 ± 0.13	^{118}Sn(d,p)	17
[34]	0.09	0.69 ± 0.17	^{118}Sn(d,p)	17
present	0	0.42 ± 0.06[a]	^{118}Sn(d,p)	12
present	0.024	0.62 ± 0.07[a]	^{118}Sn(d,p)	12
present	0.09	0.43 ± 0.08[a]	^{118}Sn(d,p)	12

[a]Average value.

TABLE VIII. Comparison of the neutron spectroscopic factors of ^{119}Sn ⊗n → ^{120}Sn$_{G.S.}$.

Ref.	E^*_{119Sn} (MeV)	SF	Reaction	E_{Lab} (MeV)
[3]	0	1.30	^{119}Sn(d,p)	15
[6]	0	0.58 ± 0.13[a]	^{120}Sn(p,d)	26.3
[6]	0.023	1.68 ± 0.35[a]	^{120}Sn(p,d)	26.3
[7]	0	1.80 ± 0.30	^{120}Sn(p,d)	20
[7]	0.023	2.40 ± 0.35	^{119}Sn(d,p)	20
[20]	0	1.30	Weak-coupling calculation	
[20]	0.023	2.0	Weak-coupling calculation	
[20]	0.023	1.80 ± 0.36	^{120}Sn$(^3$He$,\alpha)$	39
[27]	0	1.30	^{119}Sn(t,d)	4.75–5.75
[31]	0	1.47	^{119}Sn(pol d,p)	12
present	0	1.38 ± 0.22[a]	^{120}Sn(p,d)	18

[a]Average value.

TABLE IX. Comparison of the neutron spectroscopic factors of ^{120}Sn$_{G.S.}$ ⊗n → ^{121}Sn.

Ref.	E^*_{121Sn} (MeV)	SF	Reaction	E_{Lab} (MeV)
[3]	0	0.43	^{120}Sn(d,p)	15
[3]	0.006	0.21	^{120}Sn(d,p)	15
[3]	0.06	0.39	^{120}Sn(d,p)	15
[9]	0.006	0.38 ± 0.04	^{120}Sn$(\alpha,\ ^3$He$)$	187
[12]	0	0.44 ± 0.11	^{120}Sn(d,p)	17
[12]	0.006	0.49 ± 0.12	^{120}Sn(d,p)	17
[12]	0.06	0.30 ± 0.08	^{120}Sn(d,p)	17
[35]	0	0.65	^{120}Sn(t,d)	13
[35]	0.06	0.32	^{120}Sn(t,d)	13
present	0	0.37 ± 0.05	^{120}Sn(d,p)[a]	12
present	0.06	0.44 ± 0.06	^{120}Sn(d,p)[a]	12

[a]Average value.

TABLE X. Comparison of the neutron spectroscopic factors of ^{121}Sn $\otimes$n $\rightarrow$ ^{122}Sn$_{\mathrm{G.S.}}$.

Ref.	$E^*_{121\mathrm{Sn}}$ (MeV)	SF	Reaction	E_{Lab} (MeV)
[7]	0	4.5 ± 1.5	^{122}Sn(p, d)	20
[7]	0.06	1.9 ± 0.15	^{122}Sn(p, d)	20
present	0	1.59 ± 0.26[a]	^{122}Sn(p, d)	14
present	0.06	1.77 ± 0.29[a]	^{122}Sn(p, d)	14

[a]Average value.

TABLE XI. Comparison of the neutron spectroscopic factors of ^{122}Sn$_{\mathrm{G.S.}}$ $\otimes$n $\rightarrow$ ^{123}Sn.

Ref.	$E^*_{123\mathrm{Sn}}$ (MeV)	SF	Reaction	E_{Lab} (MeV)
[3]	0.025	0.43	^{122}Sn(d, p)	15
[9]	0	0.37 ± 0.04	^{122}Sn$(\alpha, {}^3\mathrm{He})$	187
[36]	0	0.38	^{122}Sn(d, p)	12
[23]	0.025	0.44 ± 0.07	^{122}Sn(d, p)	4.5–5.5
present	0	0.36 ± 0.07	^{122}Sn(d, p)[a]	12
present	0.025	0.55 ± 0.06	^{122}Sn(d, p)[a]	12

[a]Average value.

TABLE XII. Comparison of the neutron spectroscopic factors of ^{123}Sn $\otimes$n $\rightarrow$ ^{124}Sn$_{\mathrm{G.S.}}$.

Ref.	$E^*_{123\mathrm{Sn}}$ (MeV)	SF	Reaction	E_{Lab} (MeV)
[7]	0	4.5 ± 1.5	^{124}Sn(p, d)	20
[7]	0.025	3.0 ± 0.4	^{124}Sn(p, d)	20
[37]	0	5.5	^{124}Sn$({}^3\mathrm{He}, \alpha)$	205
present	0	4.82 ± 0.88[a]	^{124}Sn(p, d)	14
present	0.025	1.89 ± 0.36[a]	^{124}Sn(p, d)	14

[a]Average value.

TABLE XIII. Comparison of the neutron spectroscopic factors of ^{124}Sn$_{\mathrm{G.S.}}$ $\otimes$n $\rightarrow$ ^{125}Sn.

Ref.	$E^*_{125\mathrm{Sn}}$ (MeV)	SF	Reaction	E_{Lab} (MeV)
[3]	0.028	0.34	^{124}Sn(d, p)	15
[9]	0	0.30 ± 0.03	^{124}Sn$(\alpha, {}^3\mathrm{He})$	187
[23]	0	0.29 ± 0.04	^{124}Sn(d, p)	4.5–5.5
[23]	0.028	0.43 ± 0.06	^{124}Sn(d, p)	4.5–5.5
[38]	0	0.41 ± 0.08	^{124}Sn$(\alpha, {}^3\mathrm{He})$	65.7
[38]	0	0.42 ± 0.08	^{124}Sn(d, p)	33.3
[38]	0.028	0.44 ± 0.09	^{124}Sn(d, p)	33.3
present	0	0.25 ± 0.06	^{124}Sn(d, p)[a]	12
present	0.028	0.42 ± 0.04	^{124}Sn(d, p)[a]	12

[a]Average value.

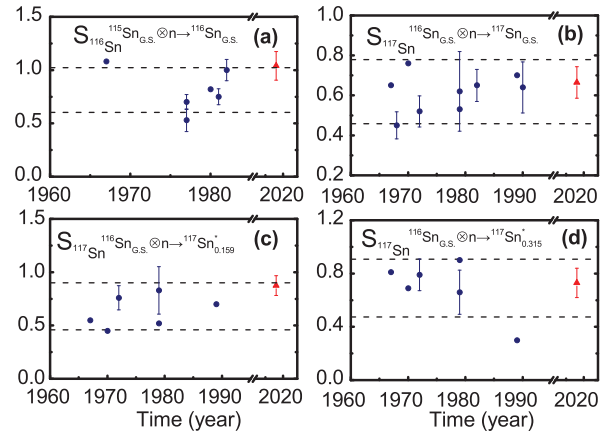

FIG. 7. The neutron spectroscopic factors of ^{116,117}Sn. The blue dots are the spectroscopic factors from the references, and the red triangle represents our result. The dotted lines show the average value region.

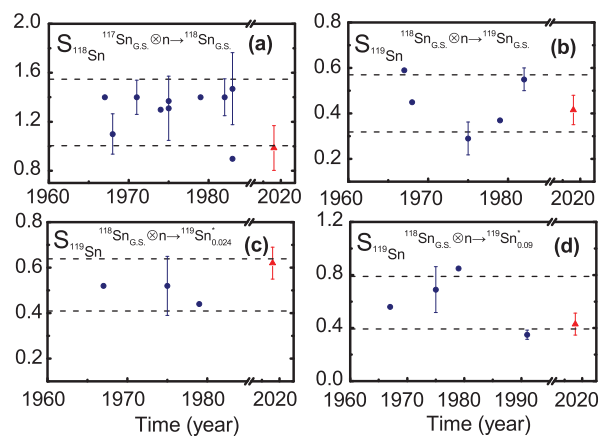

FIG. 8. The neutron spectroscopic factors of ^{118,119}Sn$_{\mathrm{g.s.}}$ and the low lying states of ^{119}Sn. The blue dots are the spectroscopic factors from the references, and the red triangle represents our result. The dotted lines show the average value region.

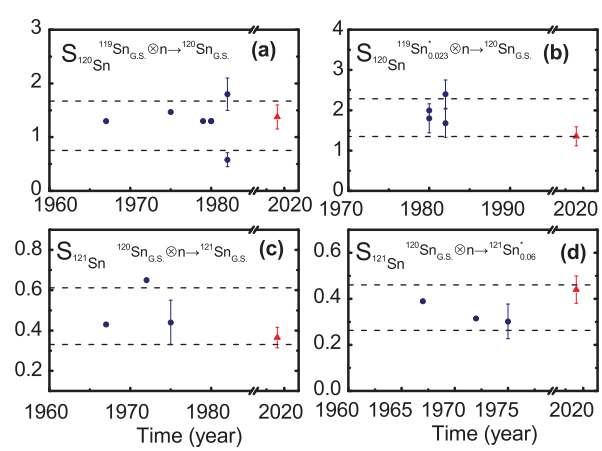

FIG. 9. The neutron spectroscopic factors of ^{120,121}Sn. The blue dots are the spectroscopic factors from the references, and the red triangle represents our result. The dotted lines show the average value region.

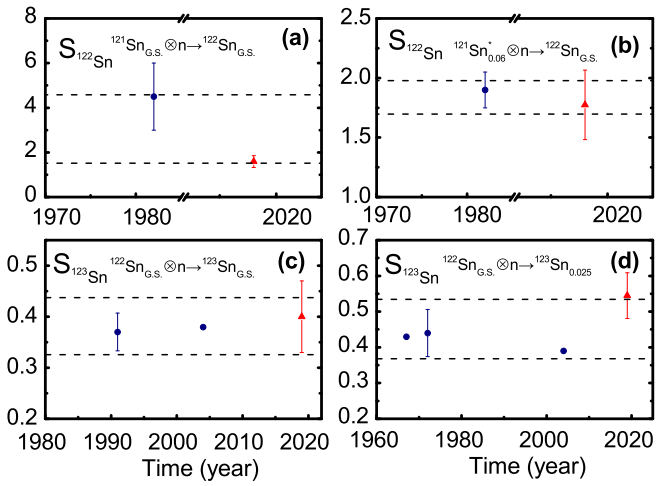

FIG. 10. The neutron spectroscopic factors of ^{122,123}Sn. The blue dots are the spectroscopic factors from the references, and the red triangle represents our result. The dotted lines show the average value region.

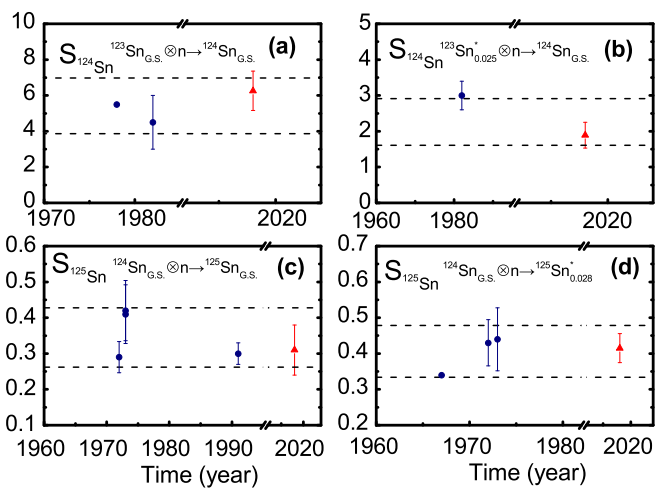

FIG. 11. The neutron spectroscopic factors of ^{124,125}Sn. The blue dots are the spectroscopic factors from the references, and the red triangle represents our result. The dotted lines show the average value region.

TABLE XIV. Neutron separation energy [$S_n(N)$], single-particle orbital angular momentum (L), $\Delta(N)$'s, and SFs.

$S_n(N)$ (MeV)	L	$\Delta_n^{(3)}(N)$ (MeV)	$\Delta_n^{(4)}(N)$ (MeV)	$\Delta_n^{(5)}(N)$ (MeV)	SF
5.705	0				0.42 ± 0.04
6.111	0				0.4 ± 0.06
6.171	0				0.37 ± 0.05
6.485	0				0.42 ± 0.06
6.945	0				0.67 ± 0.08
8.874	0	1.434	1.378	1.365	1.77 ± 0.29
9.107	0	1.468	1.39	1.392	1.38 ± 0.22
9.326	0	1.421	1.306	1.336	0.99 ± 0.18
9.563	0	1.309	1.159	1.204	1.04 ± 0.13
5.921	2				0.55 ± 0.06
6.461	2				0.62 ± 0.07
6.786	2				0.88 ± 0.09
8.514	2	1.378	1.325	1.314	1.89 ± 0.36
8.814	2	1.434	1.378	1.365	1.59 ± 0.26
9.131	2	1.468	1.39	1.392	1.36 ± 0.22
5.733	5				0.31 ± 0.07
5.946	5				0.4 ± 0.07
6.395	5				0.43 ± 0.06
6.63	5				0.73 ± 0.11
8.489	5	1.378	1.325	1.314	6.26 ± 1.1

TABLE XV. Parameters of SF $= a_0 \times S_n(N) + a_1 \times \Delta(N)$.

	L	$\Delta_n^{(3)}(N)$	$\Delta_n^{(4)}(N)$	$\Delta_n^{(5)}(N)$
a_0	0	0.07001	0.06899	0.06977
a_1	0	0.4648	0.5126	0.4982
a_0	2	0.1076	0.1072	0.1074
a_1	2	0.4587	0.4830	0.4846
a_0	5	0.07673	0.07673	0.07673
a_1	5	4.070	4.234	4.267

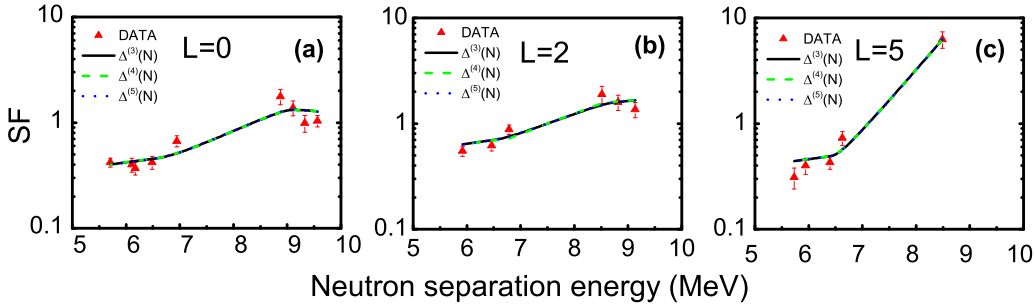

FIG. 12. SF versus neutron separation energy. The red triangles represent SFs obtained in this work. The solid lines [$\Delta_n^{(3)}(N)$], dashed lines [$\Delta_n^{(4)}(N)$], and dotted lines [$\Delta_n^{(5)}(N)$] indicate the calculated data points, not the theoretical curve.

much different from cases $L = 0$ and 2; this is likely because $L = 5$ has only one even-A Sn isotope in this work.

IV. CONCLUSIONS

Tin isotopes are extremely suitable to provide shell model information on the 50–82 neutron shell, due to the closed shell structure of protons, and the single-particle structure of nuclei in the neutron shell model can be deduced with spectroscopic factors.

In the present work, the angular distributions of (p, d) and (d, p) on $^{116,118,120,122,124}SnO_2$ targets are measured with the high resolution Q3D magnetic spectrograph. The neutron SFs of $^{116-125}$Sn are extracted by comparing the differential cross sections from experiments and DWBA calculations. The current SFs of most tin isotopes are in very good agreement with the average values of the previous works. It is worth emphasizing that our experiment has higher experimental precision and better resolution than previous works, and we identified the reaction products of adjacent energy levels of odd tin isotopes, such as $^{119}Sn_{G.S.}$ and $^{119}Sn^*_{0.024}$. But we failed to distinguish the products of $^{121}Sn_{G.S.}$ and $^{121}Sn^*_{0.006}$ for $^{120}Sn(d, p)\,^{121}Sn$ and $^{122}Sn(p, d)\,^{121}Sn$. The peaks of both reactions are contributed by the ground state, so that the SFs of the ground state are trustworthy. But for $^{120}Sn_{G.S.} \otimes n \rightarrow {}^{121}Sn_{0.006.}$ and $^{121}Sn_{0.006} \otimes n \rightarrow {}^{122}Sn_{G.S}$ the SFs obtained by different optical potentials are very different. New methods or experiments with much better resolution should be carried out to obtain accurate SFs corresponding to $^{121}Sn_{0.006}$.

A simple linear analysis of SFs with neutron separation energy $S_n(N)$ and even-A Sn pairing gap $\Delta(N)$ was done in this work, and we found that SFs are positively correlated to $S_n(N)$ and $\Delta(N)$. As $L = 5$ has just one even$-\underline{A}$Sn isotope, the parameter corresponding to $\Delta(N)$ is different from those of other L values.

ACKNOWLEDGMENTS

This work was performed with the support of the National Key Research and Development Program of China (Grant No. 2017YFF0106501), the Natural Science Foundation of Guangdong, China (Grant No. 2016A030310042), a project funded by the China Postdoctoral Science Foundation (Grant No. 2019M652999), the National Natural Science Foundation of China under Grants No. 11575118, No. 11605114, No. 11375269, and No. 11490560, the 973 Program of China under Grant No. 2013CB834406, as well as the National Key Research and Development Program of China under Grant No. 2016YFA0400502.

APPENDIX

Lohr-Haeberli [15]:

Real central potential:

$$V_r = 91.13 + 2.2(Z/A^{1/3}), \quad r_0 = 1.05, \quad a_0 = 0.86.$$

Imaginary potential:

$$W_D = 218/A^{2/3},$$

$$r_W = 1.43, \quad a_W = 0.50 + 0.013A^{2/3}.$$

Spin-orbit potential:

$$V_{so} = 7.0, \quad r_{so} = 0.75, \quad a_{so} = 0.5.$$

$$r_c = 1.3. \tag{A1}$$

Chapel-Hill 89 [16]:

Real central potential:

$$V_r = 52.9 \pm 13.1\frac{N-Z}{A} - 0.299(E - E_c),$$

$+$: proton, $-$: neutron,

$$R_0 = 1.25A^{1/3} - 0.225, \quad a_0 = 0.690,$$

$$E_c = \begin{cases} \frac{6Ze^2}{5R_c} = \frac{1.73Z}{R_c}\ \text{MeV} & \text{for } (p, p), \\ 0 & \text{for } (n, n), \end{cases}$$

$$R_c = 1.24A^{1/3} + 0.12.$$

Spin-orbit potential:

$$V_{so} = 5.9, \quad R_{so} = 1.34A^{1/3} - 1.2, \quad a_{so} = 0.63.$$

Imaginary cental potential:

$$W_v = 7.8\left[1 + \exp\left(\frac{35 - (E - E_c)}{16}\right)\right]^{-1},$$

$$W_D = \left(10 + 18\frac{N-Z}{A}\right)\left[1 + \exp\left(\frac{(E - E_c) - 36}{17}\right)\right]^{-1},$$

$$R_w = 1.33A^{1/3} - 0.42, \quad a_w = 0.690. \tag{A2}$$

Perey [17]:

Real central potential:

$$V_r = 53.3 - 0.55E + 27\frac{N-Z}{A} + 0.4(Z/A^{1/3}),$$

$$r_0 = 1.25, \quad a_0 = 0.65.$$

Imaginary surface potential: (A3)

$$W_D = 13.5 \pm 2.0, \quad r_D = 1.25, \quad a_D = 0.65.$$

Spin-orbit potential:

$$V_{so} = 7.5, \quad r_{so} = 1.25, \quad a_{so} = 0.47,$$

$$r_c = 1.25.$$

[1] D. J. Rowe, Rev. Mod. Phys **40**, 153 (1968).
[2] S. Mitsuo and K. Ken-Ichi, Nucl. Phys. A **185**, 217 (1972).
[3] E. J. Schneid, A. Prakash, and B. L. Cohen, Phys. Rev. **156**, 1316 (1967).

[4] B. Mayer, J. Gosset, J. L. Escudie, and H. Kamitsubo, Nucl. Phys. A **177**, 205 (1971).
[5] R. R. Cadmus, Jr. and W. Haeberli, Nucl. Phys. A **349**, 103 (1980).
[6] S. A. Dickey, J. J. Kraushaar, R. A. Ristinen, and M. A. Rumore, Nucl. Phys. A **377**, 137 (1982).
[7] D. G. Fleming, Can. J. Phys. **60**, 428 (1982).
[8] E. Frota-Pessôa, Nuovo Cimento A **77**, 369 (1983).
[9] C. P. Massolo, S. Fortier, S. Galès *et al.*, Phys. Rev. C **43**, 1687 (1991).
[10] M. H. Macfarlane and J. B. French, Rev. Mod. Phys **32**, 567 (1960).
[11] Jenny Lee, M. B. Tsang, and W. G. Lynch, Phys. Rev. C **75**, 064320 (2007).
[12] M. J. Bechara and O. Dietzsch, Phys. Rev. C **12**, 90 (1975).
[13] D. Y. Pang and A. M. Mukhamedzhanov, Phys. Re. C **90**, 044611 (2014).
[14] M. Igarashi, computer code TWOFNR (1977) (unpublished).
[15] J. M. Lohr and W. Haeberli, Nucl. Phys. A **232**, 381 (1974).
[16] R. L. Varner, W. J. Thompson, T. L. McAbee *et al.*, Phys. Rep. **201**, 57 (1991).
[17] F. G. Perey, Phys. Rev. **131**, 745 (1963).
[18] S. Y. Van Der Werf, M. N. Harakeh, L. W. Scholten *et al.*, Nucl. Phys. A **289**, 141 (1977).
[19] G. Berrier-Ronsin, G. Duhamel, E. Gerlic *et al.*, Nucl. Phys. A **288**, 279 (1977).
[20] E. Gerlic, G. Berrier-Ronsin, G. Duhamel, S. Galès, E. Hourani, H. Langevin-Joliot, M. Vergnes, and J. Van de Wiele, Phys. Rev. C **21**, 124 (1980).
[21] G. Perrin, G. Duhamel, C. Perrin *et al.*, Nucl. Phys. A **356**, 61 (1981).
[22] C. R. Bingham and M. L. Halbert, Phys. Rev. C **1**, 244 (1970).
[23] P. L. Carson and L. C. McIntyre, Jr., Nucl. Phys. A **198**, 289 (1972).
[24] R. R. Cadmus, Jr. and W. Haeberli, Nucl. Phys. A **327**, 419 (1979).
[25] R. C. Johnson, E. J. Stephenson, and J. A. Tostevin, Nucl. Phys. A **505**, 26 (1989).
[26] J. M. Schippers, J. M. Schreuder, S. Y. van der Werf *et al.*, Nucl. Phys. A **510**, 70 (1990).
[27] R. Chapman, M. Hyland, J. L. Durell *et al.*, Nucl. Phys. A **316**, 40 (1979).
[28] K. Yagi, Y. Saji, T. Ishimatsu *et al.*, Nucl. Phys. A **111**, 129 (1968).
[29] R. S. Mackintosh, Nucl. Phys. A **230**, 195 (1974).
[30] S. E. Vigdor and W. Haeberli, Nucl. Phys. A **253**, 55 (1975).
[31] D. C. Kocher and W. Haeberli, Nucl. Phys. A **252**, 381 (1975).
[32] Y. Aoki, H. Iida, K. Nagano *et al.*, Nucl. Phys. A **393**, 52 (1983).
[33] K. Yagi, Y. Saji, T. Ishimatsu *et al.*, J. Phys. Soc. Jpn **24**, 1167 (1968).
[34] T. Borello-Lewin, C. Q. Orsini, O. Dietzsch *et al.*, Nucl. Phys. A **249**, 284 (1975).
[35] R. F. Casten, E. R. Flynn, O. Hansen, and T. J. Mulligan, Nucl. Phys. A **180**, 49 (1972).
[36] S. Ohya, Nucl. Data Sheets **102**, 547 (2004).
[37] J. Van de Wiele, E. Gerlic, H. Langevin-Joliot *et al.*, Nucl. Phys. A **297**, 61 (1978).
[38] C. R. Bingham and D. L. Hillis, Phys. Rev. C **8**, 729 (1973).
[39] A. Bohr and B. R. Mottelson, *Nuclear Structure* (World Scientific, Singapore, 1998), Vol. 1.
[40] D. Madland and J. Nix, Nucl. Phys. A **476**, 1 (1988).
[41] S. A. Changizi, C. Qi, and R. Wyss, Nucl. Phys. A **940**, 210 (2015)